Human Molecular Genetics, 2010, Vol. 19, No. 17 **3440–3456**
doi:10.1093/hmg/ddq257
Advance Access published on June 22, 2010

The small heat shock protein B8 (HspB8) promotes autophagic removal of misfolded proteins involved in amyotrophic lateral sclerosis (ALS)

Valeria Crippa[1,5], Daniela Sau[1,5], Paola Rusmini[1,5], Alessandra Boncoraglio[1,4], Elisa Onesto[1,5], Elena Bolzoni[1,5], Mariarita Galbiati[1,5], Elena Fontana[2], Marianna Marino[3], Serena Carra[4], Caterina Bendotti[3], Silvia De Biasi[2] and Angelo Poletti[1,5,*]

[1]Dipartimento di Endocrinologia, Fisiopatologia e Biologia Applicata (Center of Excellence on Neurodegenerative Diseases, CEND) and [2]Dipartimento di Scienze Biomolecolari e Biotecnologie, Universita' degli Studi di Milano, Milano, Italy, [3]Dipartimento di Neuroscienze, Istituto di Ricerche Farmacologiche 'Mario Negri', Milano, Italy, [4]Department of Cell Biology, Section for Radiation and Stress Cell Biology, University Medical Center Groningen, Groningen, The Netherlands and [5]InterUniversity Center on Neurodegenerative Diseases (CIMN), Universita' degli Studi di Firenze, Roma 'Tor Vergata', Milano, Genova, Italy

Received May 6, 2010; Revised and Accepted June 17, 2010

Several neurodegenerative diseases, including amyotrophic lateral sclerosis (ALS), are characterized by the presence of misfolded proteins, thought to trigger neurotoxicity. Some familial forms of ALS (fALS), clinically indistinguishable from sporadic ALS (sALS), are linked to superoxide dismutase 1 (SOD1) gene mutations. It has been shown that the mutant SOD1 misfolds, forms insoluble aggregates and impairs the proteasome. Using transgenic G93A-SOD1 mice, we found that spinal cord motor neurons, accumulating mutant SOD1 also over-express the small heat shock protein HspB8. Using motor neuronal fALS models, we demonstrated that HspB8 decreases aggregation and increases mutant SOD1 solubility and clearance, without affecting wild-type SOD1 turnover. Notably, HspB8 acts on mutant SOD1 even when the proteasome activity is specifically blocked. The pharmacological blockage of autophagy resulted in a dramatic increase of mutant SOD1 aggregates. Immunoprecipitation studies, performed during autophagic flux blockage, demonstrated that mutant SOD1 interacts with the HspB8/Bag3/Hsc70/CHIP multiheteromeric complex, known to selectively activate autophagic removal of misfolded proteins. Thus, HspB8 increases mutant SOD1 clearance via autophagy. Autophagy activation was also observed in lumbar spinal cord of transgenic G93A-SOD1 mice since several autophago-lysosomal structures were present in affected surviving motor neurons. Finally, we extended our observation to a different ALS model and demonstrated that HspB8 exerts similar effects on a truncated version of TDP-43, another protein involved both in fALS and in sALS. Overall, these results indicate that the pharmacological modulation of HspB8 expression in motor neurons may have important implications to unravel the molecular mechanisms involved both in fALS and in sALS.

INTRODUCTION

Amyotrophic lateral sclerosis (ALS) is a fatal neurodegenerative disease characterized by the progressive loss of selected populations of motor neurons (1). A hallmark of ALS is the presence of insoluble material, containing proteins involved in the major intracellular degradative pathways and the human TAR DNA-binding protein TDP-43 (see below) (1,2). While the role of these inclusions is largely debated, it is generally accepted that their formation is linked to protein misfolding and may alter motor neuronal functions, impacting on their survival. Thus, by assisting protein folding, it is

*To whom correspondence should be addressed at: Dipartimento di Endocrinologia, Fisiopatologia e Biologia Applicata Universita' degli Studi di Milano, Via Balzaretti 9, 20133 Milano, Italy. Tel: +39 0250318215; Fax: +39 0250318204; Email: angelo.poletti@unimi.it

expected to reduce protein aggregation and/or other cascades of events responsible for motor neuronal cell death in ALS.

More than 80% of ALS cases are sporadic (sALS); among the rare familial forms (fALS) about one-fifth have been associated to Cu/Zn superoxide dismutase 1 (SOD1) gene mutations (3) and even less to mutations in the gene coding for TDP-43 (a protein found as a major constituent in inclusions of sALS as well as non-SOD1-fALS) (4,5). However, since sALS and fALS are clinically indistinguishable and mutant SOD1 animal and cellular models have been developed by different investigators, these models are widely used to study the disease (1). SOD1 is an essential enzyme that removes oxidant-free radical species; although many mutant SOD1s retain their enzymatic activity, a partial loss of protection from oxygen-free radicals might contribute to motor neuronal death in SOD1-linked fALS (6). However, motor neuronal death is apparently mainly due to a gain of neurotoxic function(s) related to mutant SOD1 misfolding (7).

Several studies have demonstrated that chaperones facilitate the removal of misfolded proteins. Mutations of one of these chaperones, the small heat shock protein B8 (HspB8, also called Hsp22) are responsible for distal hereditary motor neuropathy type II (dHMN) (8) and autosomal dominant Charcot–Marie–Tooth (CMT) disease type 2L (9). Interestingly, HspB8 efficiently removes misfolded proteins containing elongated polyglutamine tracts (10–12), responsible for other neurodegenerative diseases (reviewed in 13).

We have thus evaluated, in animal and cellular models, whether HspB8 may exert a protective role in ALS. The results indicate that HspB8 expression is upregulated in transgenic G93A-SOD1 (tg G93A-SOD1) mice and that HspB8 selectively removes the neurotoxic mutant SOD1 from motor neuronal cells, restoring normal proteasome activity. This action is specifically mediated by the activation of the autophagosome–lysosome pathway (APLP). HspB8 also counteracts the formation of TDP-43 aggregates. This suggests that the induction of HspB8 in motor neurons might become a novel useful target in different forms of ALS.

RESULTS

In the present study, we initially analyzed the role of HspB8 on the solubility, aggregation rate and degradation of mutant SOD1, responsible for motor neuronal cell death in some fALS patients. In a second set of experiments, we also evaluated the effect of HspB8 on TDP-43 solubility and clearance.

To this purpose, we have taken advantage of the immortalized motor neurons NSC34 cells (14). These cells are hybrid cells generated by fusion of embryonic motor neurons with neuroblastoma. We produced NSC34 cells expressing human SOD1, either wild-type (wtSOD1) or mutant (G93A-SOD1) to be used as SOD1-linked ALS models together with transgenic (tg) G93A-SOD1 mice. Both the NSC34 cells and the G93A-SOD1 mice have been extensively used in our laboratories to analyze the effects of misfolded proteins on motor neurons (6,15,16).

Mutant G93A-SOD1 aggregates and impairs the proteasome in immortalized motor neurons

The NSC34 cells expressing wt or mutant SOD1 have been analyzed to evaluate differences in the biochemical behavior of the two proteins. The data (Fig. 1A) show that wtSOD1 localized both in cytoplasm and nucleus and did not form visible aggregates. Mutant G93A-SOD1 is excluded from nuclei and forms several large intracellular aggregates. The amount of insoluble SOD1 species generated in immortalized motor neurons was quantified in the filter retardation assay (Fig. 1B) (6,16). In this assay, wtSOD1 was almost undetectable both in the basal conditions and after MG132 treatment, indicating that wtSOD1 did not aggregate even when the proteasome is impaired. Significant amounts of mutant SOD1 were instead retained on the membrane in the basal conditions, proving that the G93A mutation reduces the protein solubility. A robust increase of mutant SOD1 accumulation was observed after MG132 treatment. Western blot analyses (Fig. 1C) showed that in NSC34 cells expressing wtSOD1, the protein was in the monomeric form. The levels of wtSOD1 were only marginally increased in the presence of the proteasome inhibitor MG132. On the contrary, in NSC34 cells expressing mutant SOD1, there was a massive decrease of monomeric forms of this protein, accompanied by the formation of SDS-resistant, high M.W. species, which could represent dimeric/oligomeric forms of the misfolded mutant SOD1. The inhibition of proteasome activity resulted in a much larger accumulation of monomeric and oligomeric species (also detectable in the stacking gel). To determine whether SOD1 aggregates formed in the basal conditions or during proteasome impairment shared some biochemical similarities, we analyzed the ubiquitination pattern of mutant SOD1 expressed in NSC34 cells using two experimental approaches. Immunofluorescence microscopy data (Fig. 1D) indicated that mutant SOD1 aggregates formed in the basal condition were only marginally ubiquitinated; notably ubiquitin-positive/SOD1-negative aggregates were visible in several cells expressing the mutant SOD1. The lack of ubiquitination of mutant SOD1 aggregates was also confirmed by immunoprecipitation studies (Supplementary Material, Fig. S1A). These data are in line with our previous observations obtained using another protein prone to misfold and to aggregate, the androgen receptor (AR) containing a polyglutamine tract (ARpolyQ) responsible for an ALS-related motor neuronal disease, the spinal and bulbar muscular atrophy (SBMA or Kennedy's disease). In fact, we demonstrated that the ARpolyQ aggregation process occurs prior to (or independently of) proteasome inactivation (16). Therefore, since the clearance of the insoluble mutant SOD1 depends on the proteasome, it is expected that physiological or pathological conditions (oxidative stress, heat shock, toxic compounds etc.) able to impair proteasome functions may result in an increased intracellular accumulation of the abnormal protein, thus worsening the biochemical behavior of the protein.

To evaluate proteasome activity, NSC34 cells were co-transfected with SOD1s and the YFPu proteasome reporter protein (6,16). The results (Fig. 1E and Supplementary Material, Fig. S1B) showed that YFPu is fully degraded in immortalized motor neurons expressing wtSOD1, while it

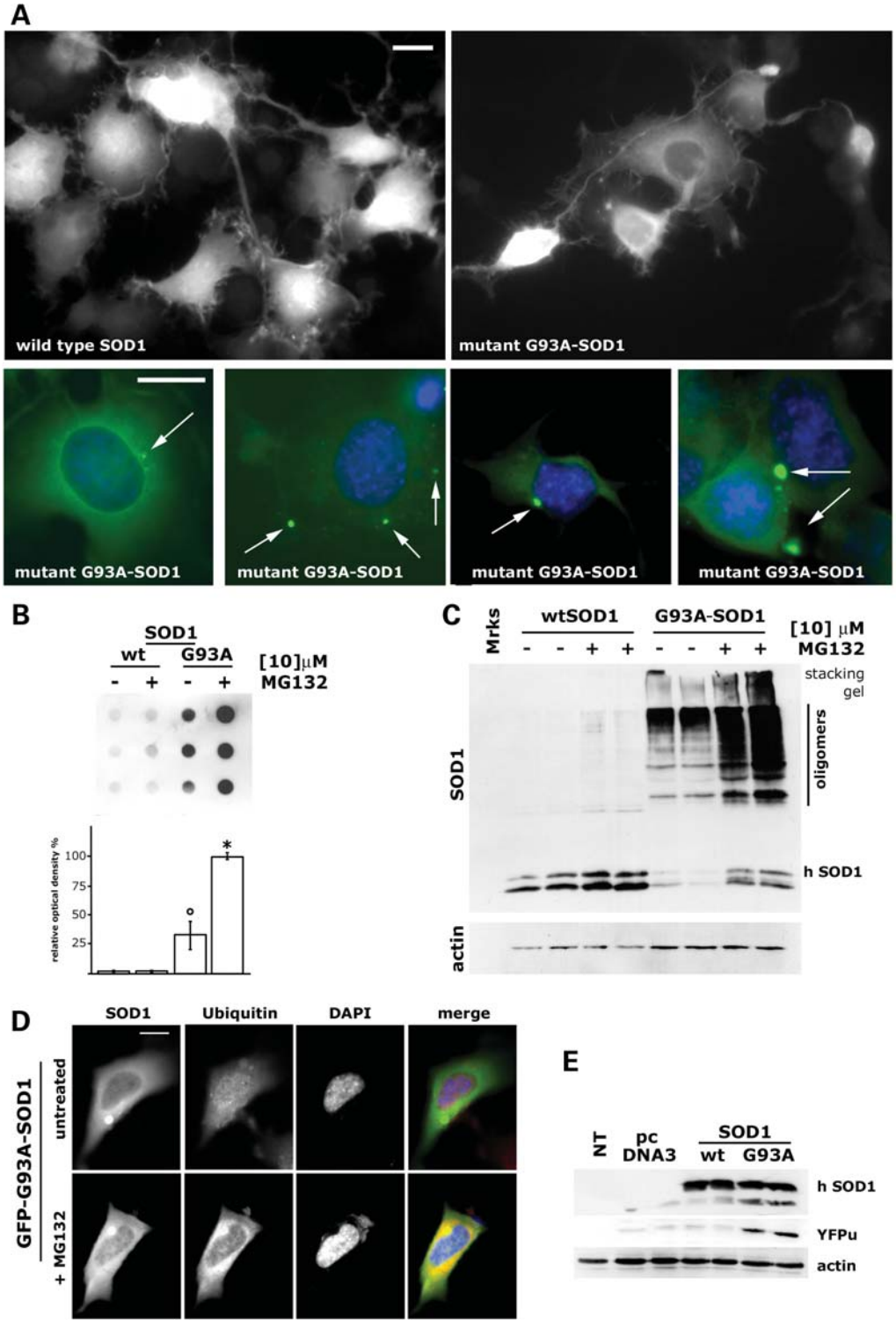

Figure 1. Biochemical behavior of wt and mutant SOD1 in motor neuronal NSC34 cells. (**A**) High-resolution fluorescent microscopy analysis on NSC34 cells transfected with GFP-wtSOD1 or GFP-G93A-SOD1. Upper insets: ×40, lower insets: ×63. Nuclei are stained with DAPI (blue). Scale bars = 10 μm. Arrows indicate mutant SOD1 aggregates. (**B**) Filter retardation assays performed on NSC34 cells transfected with wt or mutant G93A-SOD1 in the basal condition or after treatment with 10 μM of MG132 for 24 h. The histogram is obtained from optical densities of the dots from experiments performed in triplicate (mutant G93A-SOD1 versus wtSOD1 and wtSOD1+MG132, $^{\circ}P < 0.01$; mutant G93A-SOD1+MG132 versus mutant G93A-SOD1, wtSOD1 and wtSOD1+MG132, $^{*}P < 0.001$). (**C**) Western blot analyses performed on cell lysates of NSC34 cells transfected with wt or mutant G93A-SOD1 in the basal condition or after treatment with 10 μM of MG132 for 24 h. hSOD1, human SOD1 monomeric forms; oligomers, dimeric and high-molecular oligomeric species of mutant SOD1; stacking gel, SDS resistant mutant G93A-SOD1 species. (**D**) High-resolution fluorescence microscopy analysis performed on NSC34 cells transfected with GFP-G93A-SOD1 in the basal condition or after treatment with 10 μM of MG132 for 24 h and analyzed at ×63 (scale bar = 10μm). (**E**) Western blot assay performed on NSC34 cells transfected with wtSOD1 or G93A-SOD1 and YFPu. NT, untransfected cells.

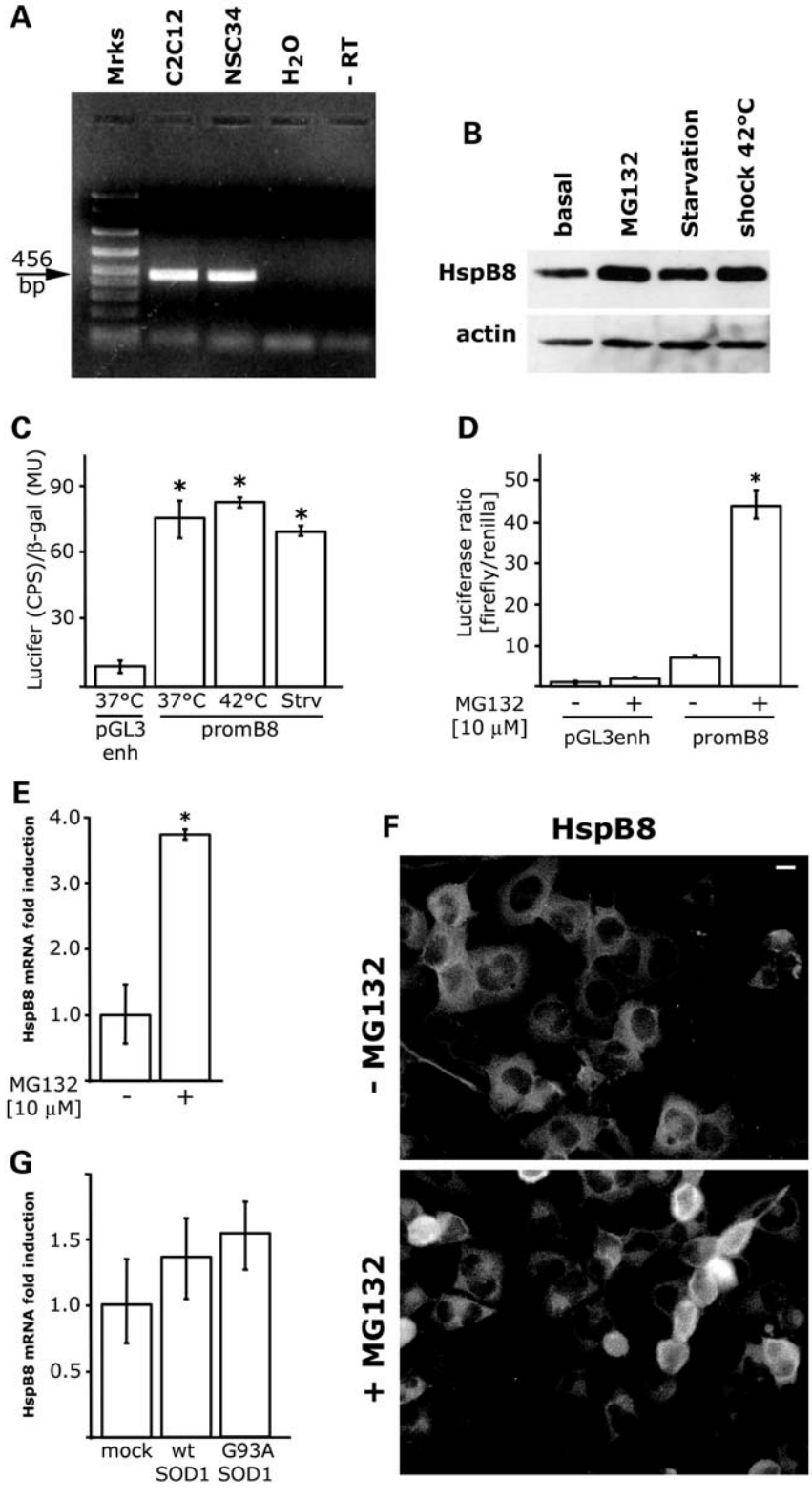

Figure 2. Effects of stress conditions on the HspB8 gene expression in motor neuronal NSC34 cells. (**A**) RT–PCR analysis to evaluate endogenous HspB8 expression in NSC34 cells. Analysis was performed on total RNA of control cultured myoblast cell line (C2C12) or motor neurons (NSC34). 456bp, HspB8 amplicon; H_2O, sample without RNA, −RT, sample without the RT-MMLV. (**B**) Western blot assay performed on NSC34 cells grown: in the basal conditions: basal, with proteasome inhibition: MG132 (10 μM for 24 h), with serum deprivation: starvation, exposed to heat shock: shock 42°C for 1 h. (**C**) Transcriptional activation of the HspB8 promoter (promB8): basal condition: 37°C, heat shock at 42°C: 42°C, serum deprivation: Strv; pGL3-enh: basal vector lacking the HspB8 promoter. Data are expressed as firefly luciferase activity (count per seconds, CPS) normalized by β-galactosidase activity (Miller Units, MU): *pGL3-enh 37°C versus promB8 37°C, 42°C and Strv, $P < 0.001$. (**D**) Effect of proteasome inhibition on the transcriptional activation of HspB8 promoter.

accumulated in cells expressing mutant SOD1, proving proteasome impairment in these cells. As expected, YFPu accumulation was greatly enhanced after MG132 treatment in cells expressing either wtSOD1 or mutant SOD1 (Supplementary Material, Fig. S1B).

Proteasome impairment activates HspB8 expression in immortalized motor neurons

The intracellular response to misfolded proteins is known to activate the chaperone systems, with the involvement of both classical heat shock proteins (Hsp70, Hsp40 etc.) and small Hsps (HspB1, HspB8 etc). The small Hsps are extremely interesting, since mutant forms of HspB1 and HspB8 have been associated with different forms of CMT type 2 disease as well as distal neuropathies (8,9,17), and the co-chaperone Bag3, the major HspB8 interactor, has been found mutated in muscular dystrophy/peripheral neuropathy (18). Moreover, HspB8 counteracts the aggregation of proteins responsible for polyQ-related neurodegenerative diseases (10). Based on these observations, we have analyzed whether HspB8 may be involved in the intracellular response to SOD1 neurotoxicity. We initially demonstrated that HspB8 is expressed in immortalized motor neuronal cells. In fact, the HspB8 mRNA was detectable (Fig. 2A) and correctly translated (Fig. 2B) in NSC34 cells. We also tested whether stressful cellular conditions, possibly implicated in sensitizing motor neurons to protein toxicity in ALS, might modify HspB8 expression levels (Fig. 2B). Serum starvation only marginally altered the HspB8 levels; greater effect was observed after heat shock. Generally, this small Hsp is poorly activated by these two insults (11,19). Interestingly, HspB8 levels dramatically increased when proteasome was impaired (with MG132), and proteasome impairment is a classical condition occurring in ALS. The HspB8 increase may depend on its accumulation (i.e. reduced degradation) or on increased gene expression (due to perturbations of the general degradative capability of the cells) (11,19). Thus, we analyzed the HspB8 promoter activity in NSC34 cells using the promB8 construct. Heat shock (42°C) or serum starvation did not modify the basal transcriptional activation of HspB8 promoter (Fig. 2C). Thus, the increased level of the HspB8 protein following heat shock was due at least in part to its reduced degradation (competition with the intracellular misfolded protein appeared after heat shock for degradation?). To determine if increased synthesis contributed to heat shock-induced elevation of HSPB8 promoter activity was assessed using the dual luciferase system (20), because the β-galactosidase levels used in the previous experiments are heavily affected by the MG132. A considerably high activation of HspB8 promoter was detectable in MG132-treated cells (5-fold over the constitutive promoter activity) (Fig. 2D). Thus, the accumulation of the HspB8 protein (Fig. 2B) is not only due to its reduced degradation, but also to a robust increase of its synthesis. The data were validated by measuring HspB8 mRNA in real-time PCR (Fig. 2E) and protein in immunocytochemistry (ICC) (Fig. 2F); both assays confirmed that HspB8 mRNA and protein levels are increased during proteasome inhibition.

Since proteasome inhibition induces HspB8 expression and mutant SOD1 over-expression results in proteasome inhibition (Fig. 1D), we analyzed the effect of mutant SOD1 on HspB8 mRNA levels in transiently or stably transfected (doxycycline inducible NSC34 cells, kindly obtained from M.T. Carrì, University of Roma 'Tor Vergata') cells. We found that, even if HspB8 mRNA expression tended to increase in the presence of the SOD1 enzyme, the protein levels were not significantly affected (Fig. 2G and Supplementary Material, Fig. S2) by SOD1s. This may also be due to the different expression system utilized.

Mutant G93A-SOD1 induces HspB8 expression in spinal cord motor neurons

We have therefore analyzed the levels of HspB8 mRNA and protein in mice models of ALS.

Initially, we analyzed possible variations of HspB8 mRNA in the spinal cord of non-transgenic (non-tg), tg wtSOD1 and tg G93A-SOD1 mice at three different disease stages: pre-symptomatic (PS), clinical symptomatic stage (CS) and end stage (ES). The real-time PCR (Fig. 3A) shows that HspB8 expression slightly declined with age in non-tg mice, being significantly lower at the oldest age (agES) corresponding to ES in tg G93A-SOD1 mice. No significant variations of HspB8 mRNA expression were present in tg wtSOD1 mice at all ages considered. Interestingly, an induction of HspB8 mRNA expression was detectable in ES tg G93A-SOD1 mice compared with PS or CS tg G93A-SOD1 mice, and to the corresponding agES tg wtSOD1 mice. Overall, the data strongly suggest that a partial de-protection against neurotoxicity of the misfolded proteins might take place with the aging processes in normal animals, since the levels of HspB8 decrease in adulthood. However, a considerable response to the presence of mutant SOD1 was activated in older animals, indicating that spinal cord cells tended to improve their ability to respond to misfolded proteins, in line with data obtained in NSC34 cells in which proteasome impairment induced HspB8 over-expression.

Immunohistochemistry analysis of the HspB8 protein showed a weak and diffuse staining in lumbar spinal cord sections of non-tg and tg wtSOD1 mice at all ages (Fig. 3Ba–f, and Supplementary Material, Fig. S3A and B). In ES tg G93A-SOD1 mice, an intense labeling was evident, particularly in the ventral horn, in areas containing the lateral and medial motor neuronal pools, in white matter and in the ventral root exit zone (Fig. 3Bg). This was confirmed at higher magnification where motor neurons can be better

The data reported are expressed as firefly luciferase activity normalized by renilla luciferase activity. *promB8 versus promB8+MG132, $P < 0.001$. (**E**) Real-time PCR on endogenous HspB8 mRNA in motor neurons with or without 24 h of proteasome inhibition (*$P < 0.001$). (**F**) Immunofluorescence analysis on endogenous HspB8 in motor neurons with or without 24 h of proteasome inhibition. Images taken at ×10 (scale bar = 10μm). (**G**) Real-time PCR showing the effects of wt and G93A-SOD1 expression on endogenous HspB8 mRNA levels in motor neurons. Mock, NSC34 transfected with pcDNA3; wtSOD1, NSC34 transfected with pcDNA3-wtSOD1; G93A-SOD1, NSC34 transfected with pcDNA3-G93A-SOD1.

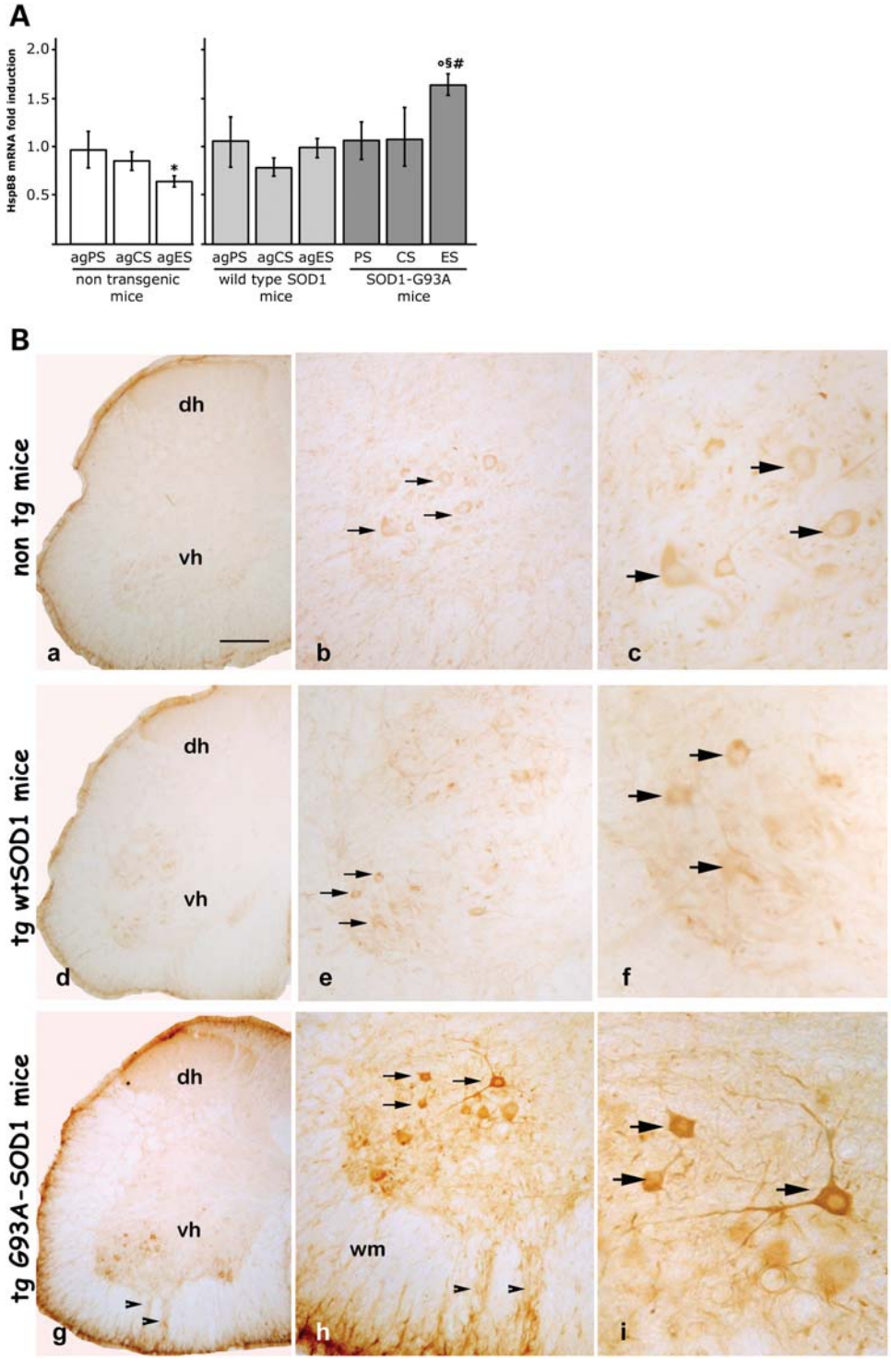

Figure 3. HspB8 expression in an animal model of ALS. (**A**) Real-time PCR on HspB8 mRNA expression levels in lumbar spinal cord of non-tg mice, tg wt SOD1 mice and tg G93A-SOD1 mice. ag, age-matched non-tg mice or tg wt SOD1 mice compared with tg G93A-SOD1 mice [PS animals (11 weeks); CS, clinical symptomatic stage (18 weeks); ES (24 weeks)]. Non-tg mice agES versus non-tg mice agPS, $^{*}P < 0.05$; tg G93A-SOD1 mice ES versus tg wtSOD1 mice agCS, $^{\circ}P < 0.001$; versus tg wtSOD1 mice agPS, agES and tg G93A-SOD1 mice PS, $^{\S}P < 0.01$; tg G93A-SOD1 mice ES versus tg G93A-SOD1 mice CS ($^{\#}P < 0.05$). (**B**) Immunohistochemical localization of HspB8 in lumbar spinal cord sections of non-tg mice (a–c) and of tg wtSOD1 mice (d–f) or tg G93A-SOD1 mice (g–i) at 22 weeks of age (ES). Figures (a), (d) and (g) are low magnifications of spinal cord hemisections (dh, dorsal horn; vh, ventral horn; scale bar = 27 μm); figures (b), (e) and (h) are details of the ventral horn (scale bar = 10 μm) and figures (c), (f) and (i) are high magnifications of motor neurons (scale bar = 4 μm). Arrows point to labeled motor neurons. In control, non-tg and tg wtSOD1 mice HspB8 is weekly expressed in the spinal cord (a and d) and motor neurons (arrows in b, c, e and f) display only a faint immunoreactivity in their soma and proximal dendrites. In tg G93A-SOD1 mice (g–i), HspB8 is more intensely expressed compared with controls and it is evident in the neuropil of ventral horn, in the soma and proximal dendrites of motor neurons (arrows in h and i), in motor neuronal axons (arrowheads in g and h point to the ventral root exit area) and in the white matter (wm).

appreciated (Fig. 3Bb, c, e, f, h, i). Motor neurons of control non-tg and tg wtSOD1 mice showed only a faint labeling in their soma and proximal dendrites (Fig. 3Bb, c, e, f and Supplementary Material, Fig. S3A and B), whereas in the ventral spinal cord of tg G93A-SOD1 mice HspB8 immunoreactivity was present both in the neuropil and in the soma and proximal dendrites of motor neurons (Fig. 3Bh and i). In spinal cord sections of PS and CS tg G93A-SOD1 mice, only a moderate increase in HspB8 immunoreactivity was found in ventral horn compared with controls (Supplementary Material, Fig. S3A–D).

The possible co-localization of mutant SOD1 with HspB8 in the lumbar spinal cord was analyzed in immunofluorescence confocal microscopy. In line with the immunoperoxidase data (Fig. 3), HspB8 was poorly expressed in motor neurons of tg wtSOD1 mice (Fig. 4A–A′), whereas in tg G93A-SOD1 mice at PS age, HspB8 labeling was intense only in motor neurons accumulating human SOD1, and weak in motor neurons containing low levels of human SOD1 (Fig. 4B–B′). In tg G93A-SOD1 mice at ES, HspB8 was intensely expressed in several motor neurons containing human SOD1 and also in the neuropil (Fig. 4C–C′). Moreover, immunofluorescence double-labeling with anti-GFAP to visualize astrocytes showed that only in spinal cord sections of ES tg G93A-SOD1 mice the reactive astrocytes in ventral gray and white matter also expressed HspB8 (Fig. 4D–E). On the contrary, microglial cells identified with the lectin LEA did not express HspB8 (Supplementary Material, Fig. S3E).

These data support the idea that HspB8 is over-expressed selectively in motor neurons that are more sensitive to mutant SOD1 neurotoxicity and in the numerous activated astroglial cells present only in ES tg G93A-SOD1 mice. Thus, the lack of a detectable increase in HspB8 mRNA levels at the PS stage (Fig. 3A) could be explained by a restricted increase of HspB8 expression in motor neurons, undetectable in real-time PCR performed on whole spinal cord samples.

HspB8 expression increases the clearance and removes mutant G93A-SOD1 oligomers and aggregates in immortalized motor neurons via a proteasome-independent pathway

Because of the biological action of chaperone proteins, we tested the possibility that HspB8 modifies the mutant SOD1 solubility, the aggregation rate and/or the ability of the proteasome to remove insoluble species in NSC34 cells co-expressing wt or mutant SOD1 and HspB8. Fluorescence analysis (Fig. 5A) showed that, in the basal conditions, mutant SOD1 formed intracellular aggregates that are completely removed by HspB8; a massive decrease of mutant SOD1 protein levels was also detectable, suggesting that this chaperone activates SOD1 degradation. Moreover, while the levels of mutant SOD1 were negligible in HspB8-expressing motor neurons, no variations in the levels and cellular distribution of wtSOD1 were detectable (Fig. 5A). The quantitative analysis (Table 1 in Fig. 5B) showed that HspB8 expression reduced both the total number of cells containing aggregates and the mean aggregates per cell.

Figure 5C shows the effects of HspB8 on the solubility of mutant SOD1 in immortalized motor neurons. The over-expression of HspB8 completely removed SDS-resistant high M.W. oligomers of mutant SOD1 and increased the clearance of the full-length mutant monomer. Interestingly, HspB8 also efficiently acted on mutant SOD1 expressed in NSC34 cells with MG132-induced proteasome impairment. Similar data were obtained by measuring the total levels of insoluble mutant SOD1 by filter retardation assay (Fig. 5C, bottom inset). In fact, HspB8 efficiently counteracted the formation of the total amount of mutant SOD1 insoluble species, confirming that the mutant misfolded SOD1 protein is cleared by an intracellular degradative system in an HspB8-dependent/proteasome-independent manner.

The analysis of the biochemical behavior of mutant SOD1 insoluble aggregates tested in buffers with increasing detergent properties showed that HspB8 over-expression almost completely counteracted the formation of all types of mutant SOD1 insoluble species (PBS-, Triton-, SDS- and Formic Acid-resistant) both the monomeric and high M.W. species (Supplementary Material, Fig. S4A–D). These data further support the notion that HspB8 acts also when proteasome is impaired. In fact, it clearly appears both from Fig. 5C and D and Supplementary Material, Fig S4 that most of the detergent-resistant high M.W. species were removed by HspB8 even in the presence of MG132. Interestingly, when the proteasome was inhibited by MG132, the HspB8 was found in a triton-resistant, SDS soluble form (Supplementary Material, Fig. S4C). The biological meaning of this observation remains to be elucidated. These effects were not due to HspB8-induced modifications of cell growth and survival, since cell viability tests showed no variation in NSC34 cells over-expressing HspB8 and wt or mutant SOD1 (Supplementary Material, Fig. S5). Moreover, the data also demonstrated that HspB8 over-expression facilitated the clearance of the misfolded protein, without generating neurotoxic (oligo/eteromeric) species from mutant SOD1 aggregate processing. Cell viability data also exclude compensatory mechanisms generating excessive activation of deleterious processes (i.e. autophagic cell death/cell self-cannibalism and apoptotic mechanisms, both reported in neurodegeneration).

The effect of HspB8 on proteasome activity in G93A-SOD1/NSC34 cells is shown in Figure 5D. In NSC34 cells expressing mutant SOD1, YFPu accumulation was completely counteracted by the contemporary expression of HspB8, an effect evident also in the presence of MG132. Thus, HspB8-induced mutant SOD1 solubility did not affect proteasome activity in immortalized motor neurons (as it may be expected by the increased amount of the misfolded proteins to be processed).

Therefore, we wanted to evaluate whether the HspB8 action on the mutant SOD1 protein is specifically mediated by its chaperone properties. To this purpose, we have taken advantage of the existence of two HspB8 mutants (K141N or K141E); these HspB8 mutants are associated with the development of HMN and/or CMT (8,9) and characterized by a marked reduction of their chaperone activity. We initially evaluated the effects of either wt or mutant HspB8s on the total levels of mutant SOD1 by using a GFP-tagged G93A-SOD1 in flow cytofluorimetric analysis. The results

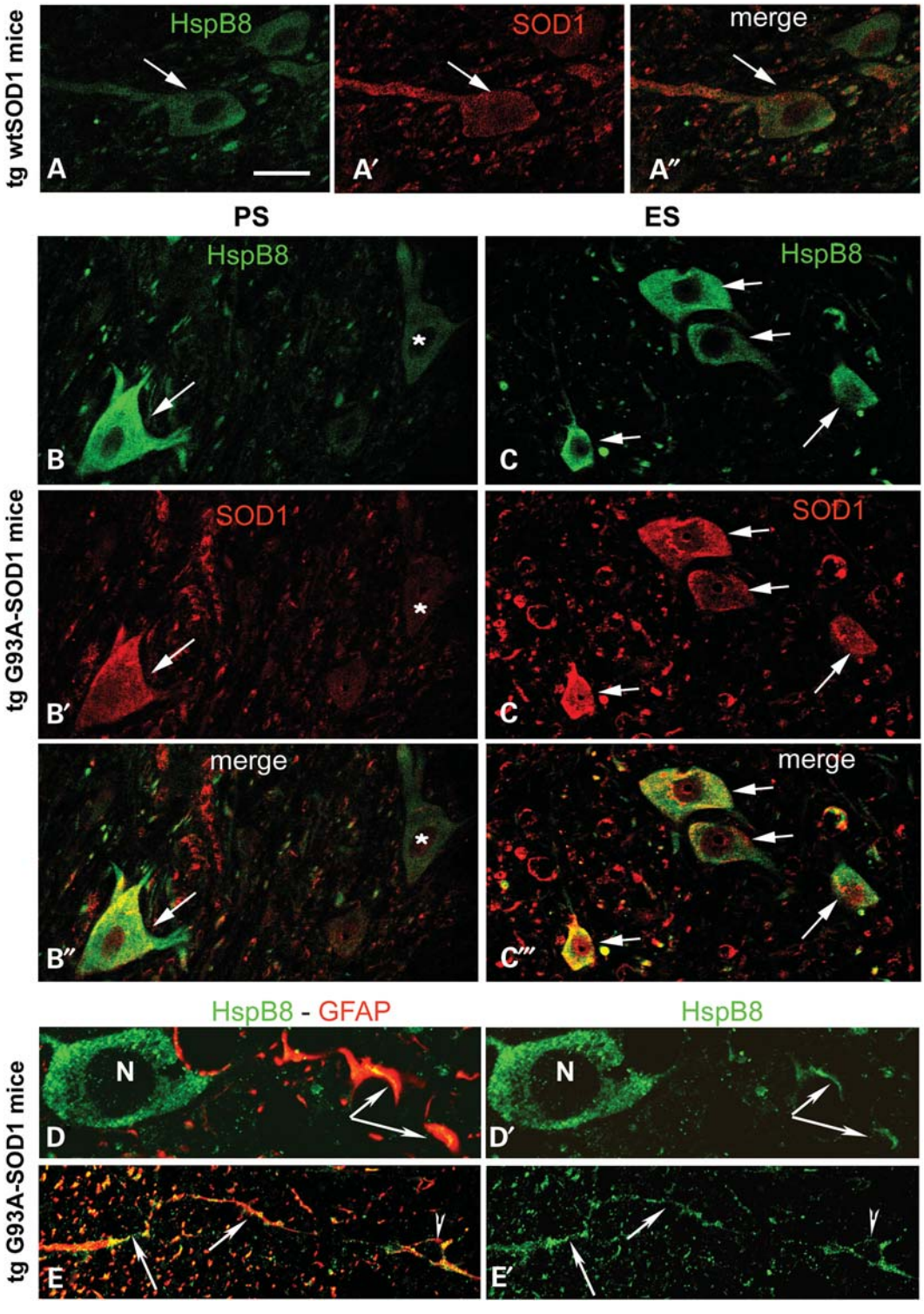

Figure 4. HspB8, G93A-SOD1 and GFAP localization in the lumbar spinal cord of a mouse model of ALS. (**A**–**C**′) HspB8 and G93A-SOD1 in anterior horn motor neurons. Immunofluorescent localization of HspB8 (green) and human SOD1 (red) in ventral lumbar spinal cord sections of age-matched ES tg wtSOD1 mice (A–A′) and of pre-symptomatic (PS, B–B′) and ES (C–C′) tg G93A-SOD1 mice. In tg wtSOD1 mice (A–A′), HspB8 is weekly expressed in the soma and proximal dendrites of motor neurons containing moderate amounts of SOD1 (arrows). In tg G93A-SOD1 mice at PS (b–b′), HspB8 is intensely expressed only in motor neurons containing human SOD1 (arrows) and weekly expressed in motor neurons (asterisks) not containing human SOD1. In tg G93A-SOD1 mice at ES (C–C′), HspB8 is intensely expressed in several motor neurons containing human SOD1 (arrows) and also in the neuropil. Scale bar = 3 μm. (**D**–**E**′) HspB8 and GFAP in ventral spinal cord. Both in the gray matter (D–D′) and in the white matter (E–E′) some GFAP-labeled astrocytic processes (arrows) and cell bodies (arrowhead) express HspB8 immunoreactivity. *N*, HspB8-positive motor neuron. Scale bar = 2 μm.

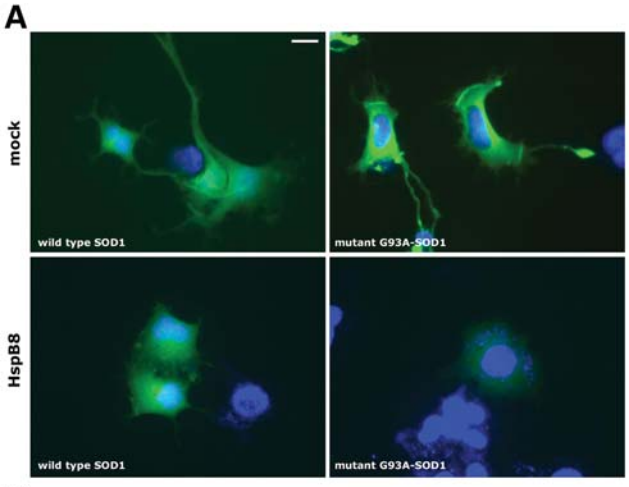

B

Table 1 - SOD1-G93A aggregates on total transfected cells			
total number of cells containing SOD1-G93A aggregates			
		% of cells containing SOD1 aggregates	number of SOD1 aggregates/cells
basal	mean±S.D.	50.47±8.43	5.36±1.34
+HspB8	mean±S.D.	18.91±8.19 *	1.94±0.76 °

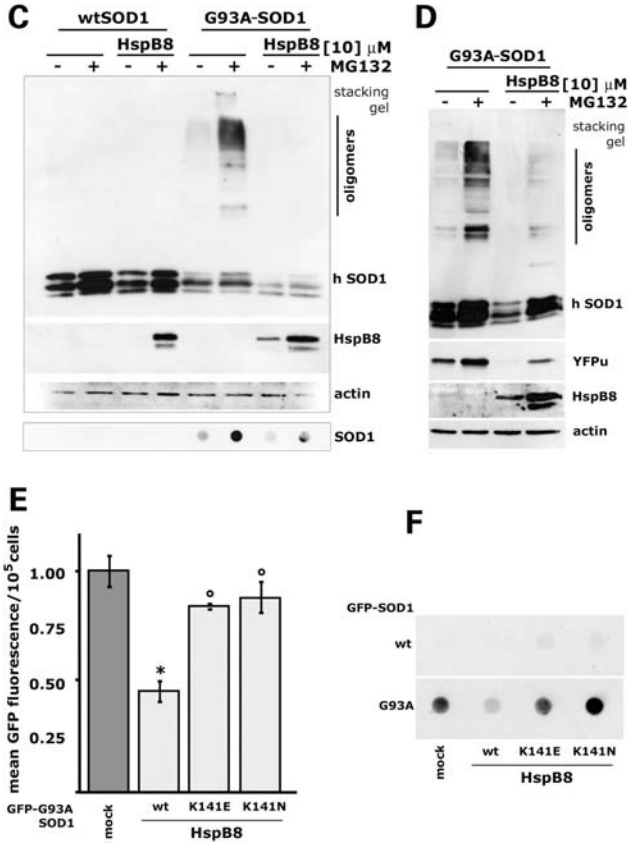

Figure 5. Effects of HspB8 on mutant G93A-SOD1 aggregation, solubility and degradation, as well as on proteasome functions in motor neuronal NSC34 cells. (**A**) Fluorescent microscopy (40×) analysis on motor neurons expressing HspB8 and either GFP-wtSOD1 or GFP-G93A-SOD1. Scale bar = 10μm. (**B**) Quantification of HspB8 effects on the number of SOD1 aggregates in NSC34 cells. Number of SOD1 aggregates positive cells basal versus +HspB8, $^{*}P < 0.0001$; mean SOD1 aggregates number per cell basal versus +HspB8, $^{\circ}P < 0.00001$. (**C**) Western blot analyses (top) on NSC34 expressing HspB8 and either wt or G93A-SOD1s with or without proteasome inhibition. hSOD1, human SOD1 monomeric forms; mSOD1, mouse SOD1; oligomers, mutant SOD1 dimeric and high molecular weight (MW) species. Filter retardation assay (bottom) performed on the same samples. (**D**) Western blot assay on NSC34 cells expressing G93A-SOD1 and YFPu with or without HspB8 and 24 h of proteasome inhibition. (**E**) Flow cytofluorimetric analysis performed on NSC34 expressing GFP tagged mutant G93A-SOD1 (GFP-G93A-SOD1) alone or co-transfected with either HspB8 or mutant HspB8 lacking chaperone activity (HspB8 carrying the K141E or K141N mutations) (GFP-G93A-SOD1+HspB8 versus GFP-G93A-SOD1, $^{*}P < 0.001$; GFP-G93A-SOD1+HspB8_K141E or K141N versus GFP-G93A-SOD1+HspB8, $^{\circ}P < 0.001$). (**F**) Filter retardation assays performed on NSC34 cells co-transfected with wt or mutant GFP-G93A-SOD1 and either the wtHspB8 or the HspB8 carrying the K141E or K141N mutations.

(Fig. 5E) demonstrate that HspB8 greatly reduced the total levels of GFP-G93A-SOD1 ($P < 0.001$). When K141E or K141N variants of HspB8 were used, the total levels of mutant GFP-G93A-SOD1 remained unchanged, and the effect of wtHspB8 was lost ($P < 0.001$). To prove that the chaperone activity is specifically directed toward misfolded SOD1 forms prone to aggregation, we have analyzed the effects of the same HspB8 variants on the insoluble mutant SOD1 species trapped by cellulose acetate membranes in a filter retardation assay. The results (Fig. 5F) demonstrate that only the wtHspB8, which retains its chaperone activity, counteracted the formation of mutant SOD1 insoluble species in immortalized motor neurons; instead, comparable levels of insoluble mutant GFP-G93A-SOD1 aggregates were present in mock transfected NSC34 cells and in those expressing HspB8 K141 mutants lacking the chaperone activity. The data strongly suggest that HspB8 chaperone activity is absolutely required to remove mutant SOD1 from our immortalized motor neuronal NSC34 cells.

HspB8 induces mutant G93A-SOD1 clearance by activating the autophagosome–lysosome pathway

Since the HspB8-dependent removal of insoluble forms of mutant SOD1 does not require a functional proteasome, we further analyzed whether the autophagic system might be the cellular pathway responsible for the beneficial effects of HspB8 on misfolded proteins involved in ALS. In fact, there are consistent molecular evidences demonstrating that APLP removes aggregated proteins (21), and HspB8, after interaction with Bag3, activates autophagy (11,19,22,23,36). We thus evaluated the effects of HspB8 on the clearance of the misfolded mutant SOD1 via the APLP (24). Initially, we analysed HspB8 activation of APLP by electron miscroscopy in NSC34 cells. In the cytoplasm of NSC34 cells expressing HspB8 together with G93A-SOD1 (Fig. 6Aa–c) or wtSOD1 (Supplementary Material, Fig. S6A–C), we detected numerous vesicles of different sizes surrounded by a double membrane, thus identifiable as autophagosomes, which were absent in NSC34 cells without HspB8. Moreover, electron microscopy of the ventral spinal cord of ES tg G93A-SOD1 mice revealed the presence of intraneuronal autophagosome-like vesicles (Fig. 6Ad and e), whereas motor neurons of agES tg wtSOD1 mice contained only lypofuscin (Supplementary Material, Fig. S6D and E). This

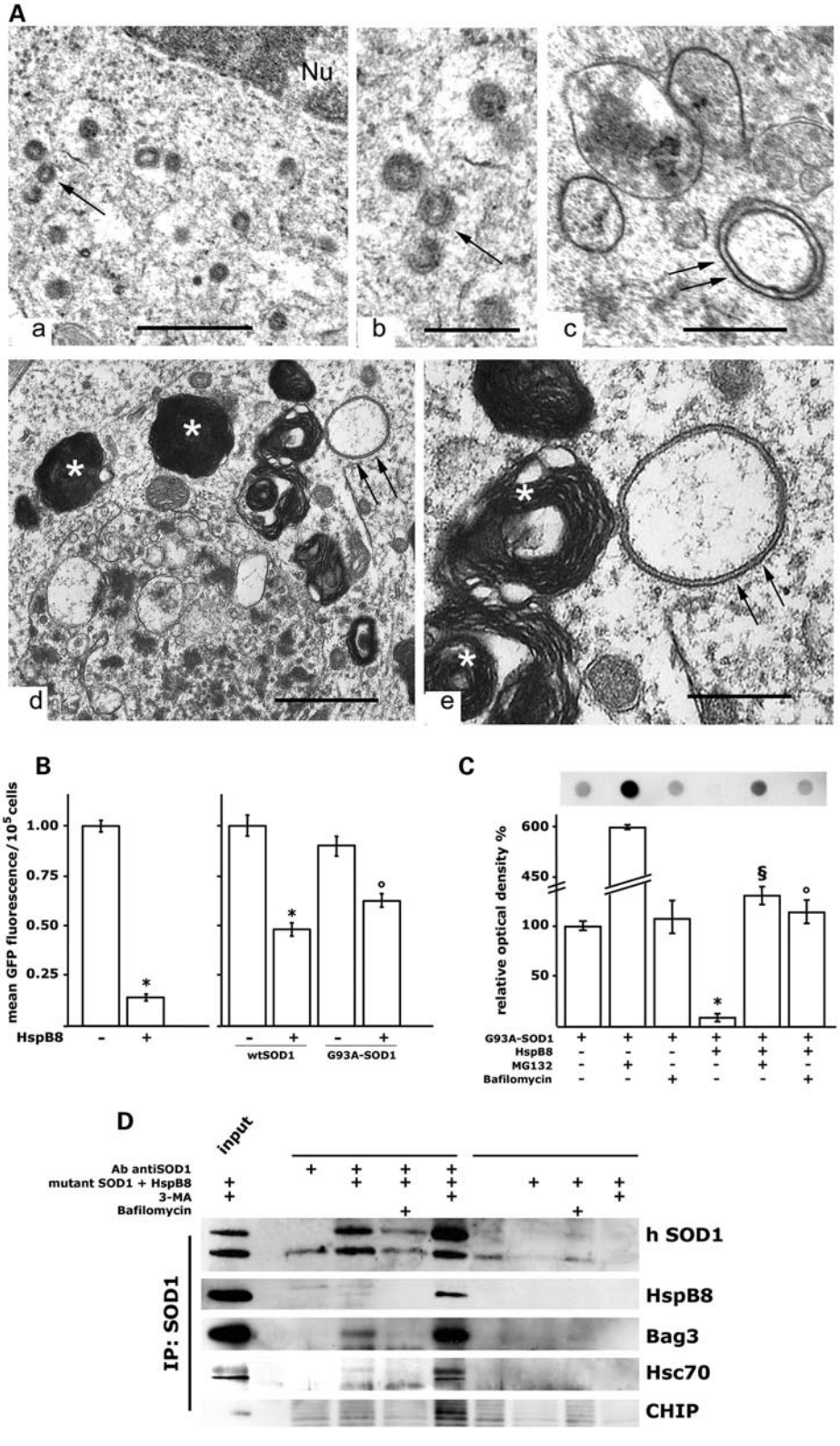

Figure 6. Effects of HspB8 on autophagic marker accumulation in motor neuronal NSC34 cells. (**A**) Ultrastructural detection of autophagic structures in NSC34 cells transfected with G93A-SOD1 and HspB8 (a–c) and in lumbar spinal cord sections of tg G93A-SOD1 mice at ES (d and e). The cytoplasm of NSC34 double-transfected cells contains several vesicles of different sizes surrounded by a double membrane (arrows); Nu, nucleus. Scale bars = 0.5 μm in (a) and (c); 0.2 μm in (b). The cytoplasm of neuronal profiles in ES tg G93A-SOD1 mice contains vacuoles surrounded by a double membrane (arrows) dispersed among aggregates of electron-dense material and whorls of membrane-like structures (asterisks). Scale bars = 2 μm in (d); 1 μm in (e). (**B**) Flow cytofluorimetric analysis performed on NSC34 cells expressing GFP-LC3 and either wtSOD1 or mutant G93A-SOD1. Cells have been synchronized at APLP for 15 h

suggests that surviving motor neurons in fALS mice can activate autophagy.

Fluorescence microscopy (Supplementary Material, Fig. S7) showed that HspB8 over-expression greatly accelerates LC3 turnover, as indicated by a general decrease of transfected GFP-LC3 in the vast majority of NSC34 cells (upper insets). At higher resolution, the NSC34 cells expressing HspB8 and still containing fluorescence showed the classical intense LC3 punctate distribution, proving that this autophagic marker is bound to the autophagosome membrane as an LC3-II lipidated isoform. On the contrary, GFP-LC3 cells not expressing HspB8 showed a more intense, but diffuse cytoplasmic distribution of the fluorescence, indicating that in this condition the autophagic marker is in the soluble LC3-I inactive form, not bound to autophagosome membranes.

To quantify the effect of HspB8 on autophagy and to further characterize the APLP involvement in ALS models, we adopted a bafilomycin-synchronized APLP protocol (24) to measure, by flow cytofluorimetric analysis, LC3 turnover in a limited time window of observation. The experiments (Fig. 6B and C) performed on G93A-SOD1 NSC34 cells showed that HspB8 dramatically decreased the intracellular levels of LC3, in only 3 h of active APLP. To prove that HspB8 acts via the APLP system, we performed filter retardation assays on cell lysates of NSC34 cells expressing mutant GFP-G93A-SOD1 and treated with the APLP inhibitor bafilomycin (Fig. 6C). The data confirmed that HspB8 induced a dramatic reduction (about 5–6-fold) of the total insoluble species even in the presence of MG132. The results demonstrated that bafilomycin counteracted the HspB8-induced clearance of the insoluble species formed by the misfolded mutant SOD1 protein. We further investigated the potential mechanism of action of HspB8 in activating mutant SOD1 degradation via autophagy, by looking at possible interactions between the two proteins. Surprisingly, immunoprecipitation studies, using an anti-SOD1 antibody, showed that in the basal condition HspB8 did not directly interact with SOD1 (Supplementary Material, Fig. S8A). In MG132-treated NSC34 cells, SOD1 enzymes co-immunoprecipitated with small amounts of HspB8 (Supplementary Material, Fig. S8B). This suggests that the perturbation of the ubiquitin-proteasome pathway may result in a general accumulation of the HspB8 client proteins to be degraded.

We thus postulated that the lack of interaction between mutant SOD1 and HspB8 could be due to the fast degradation of the mutant SOD1 when it is recognized by the HspB8, since HspB8 efficiently targets mutant SOD1 for autophagic clearance. Obviously, because of its nature, the mutant SOD1/HspB8 complex will be characterized by a very short half-life, being quickly removed by autophagy. We thus speculated that a blockage of autophagy should induce accumulation of the HspB8/SOD1 complex. To this purpose, we adopted different experimental paradigms in which (i) we blocked autophagy initiation using 3-MA, to try to prevent HspB8/SOD1 dissociation and degradation, (ii) we allowed autophagy initiation, but blocked autophagosome–lysosome full activation using bafilomycin. This might allow the release of mutant SOD1 from HspB8, and its insertion into the autophagic machinery. The results obtained (Fig. 6D) perfectly overlap our working model. In fact, when autophagy-mediated clearance of mutant SOD1 was pharmacologically blocked with 3-MA, we were able to detect co-immunoprecipitation of mutant SOD1 with HspB8. We also included in this analysis the immunodetection of Bag3, Hsc70 and CHIP. In fact, it has very recently been demonstrated that misfolded proteins are recognized by HspB8 and then inserted in a multiheteromeric complex, which includes HspB8, Bag3, Hsc70 and CHIP, that allow p62 recognition of the target protein and the formation of the autophagosome (25). The immunoprecipitation performed using an anti-SOD1 antibody on untreated 3-MA- or bafilomycin-treated NSC34 neurons expressing mutant SOD1 showed the presence of a faint band of HspB8 or of Bag3 in the basal conditions, when misfolded SOD1 was recognized and immediately targeted for autophagic degradation. Autophagy blockage with 3-MA prevents autophagosome assembly, and misfolded mutant SOD1 cannot be inserted into the autophagosome. The misfolded SOD1 was not cleared from the cell and co-immunoprecipitated with HspB8, Bag3, Hsc70 and CHIP, in the multiheteromeric complex required for misfolded protein insertion into the autophagosome.

Autophagy blockage with bafilomycin did not prevent the autophagosome assembly. In these conditions, the misfolded mutant SOD1 can be inserted into the autophagosome, and is obviously released from the HspB8/Bag3/Hsc70/CHIP complex. Since all these proteins co-immunoprecipitate with misfolded SOD1 when its insertion into the autophagosome is prevented with 3-MA, HspB8 activity in motor neurons is directly responsible for autophagic removal of mutant SOD1. Since HspB8 over-expression is sufficient to re-activate mutant SOD1 autophagic clearance, the HspB8 in this view might act as a limiting factor of the entire degradative pathway.

HspB8 chaperone effects assist the removal of TDP-43 insoluble species and aggregates via autophagy

Recently, most sALS and several fALS have been linked to the presence of inclusions positive for the TDP-43 protein

using 10 nM of bafilomycin, which was removed 3 h prior to the analysis (mock versus mock+HspB8, wtSOD1 versus wtSOD1+HspB8, $^{*}P < 0.001$; G93A-SOD1 versus G93A-SOD1 + HspB8, $^{\circ}P < 0.01$). (**C**) Filter retardation assays on NSC34 cells expressing mutant GFP-G93A-SOD1 in the absence or presence of HspB8, in the basal condition or after treatment with 10 μM of MG132 for 24 h, or 10 nM of Bafilomycin for 24 h. The histogram represents a quantification of the filter retardation assay (from three different replicates) ($^{*}P < 0.001$, +HspB8 versus −HspB8; $^{\S}P < 0.001$, +Mg132+HspB8 versus +Mg132; $^{\circ}P < 0.001$, +HspB8+bafilo versus +HspB8). (**D**) Analysis of the interaction between mutant SOD1s and HspB8 in immortalized motor neurons during autophagy blockage. Western blot analysis is performed on SOD1 immunoprecipitated samples obtained from untransfected NSC34 or NSC34 expressing mutant G93A-SOD1 in the presence of HspB8. The blot was subsequently processed using an anti-SOD1 antibody and after stripping processed with anti-c-myc antibody recognizing transfected HspB8, anti-Bag3 antibody, anti-Hsc70 antibody and finally anti-CHIP antibody (the antibodies against Bag3, Hsc70, CHIP recognize the endogenous mouse proteins). Treatments were performed using 10 mM 3-MA for 24 h or 10 nM of bafilomycin for 24 h. It appears that a faint band of HspB8 is present in immunoprecipitated samples of mutant SOD1 in the basal conditions. Inhibition of autophagosome formation with 3-MA, resulted in a dramatic accumulation of the complex known to mediate the HspB8 action through autophagy: HspB8-Bag3-Hsc70-CHIP.

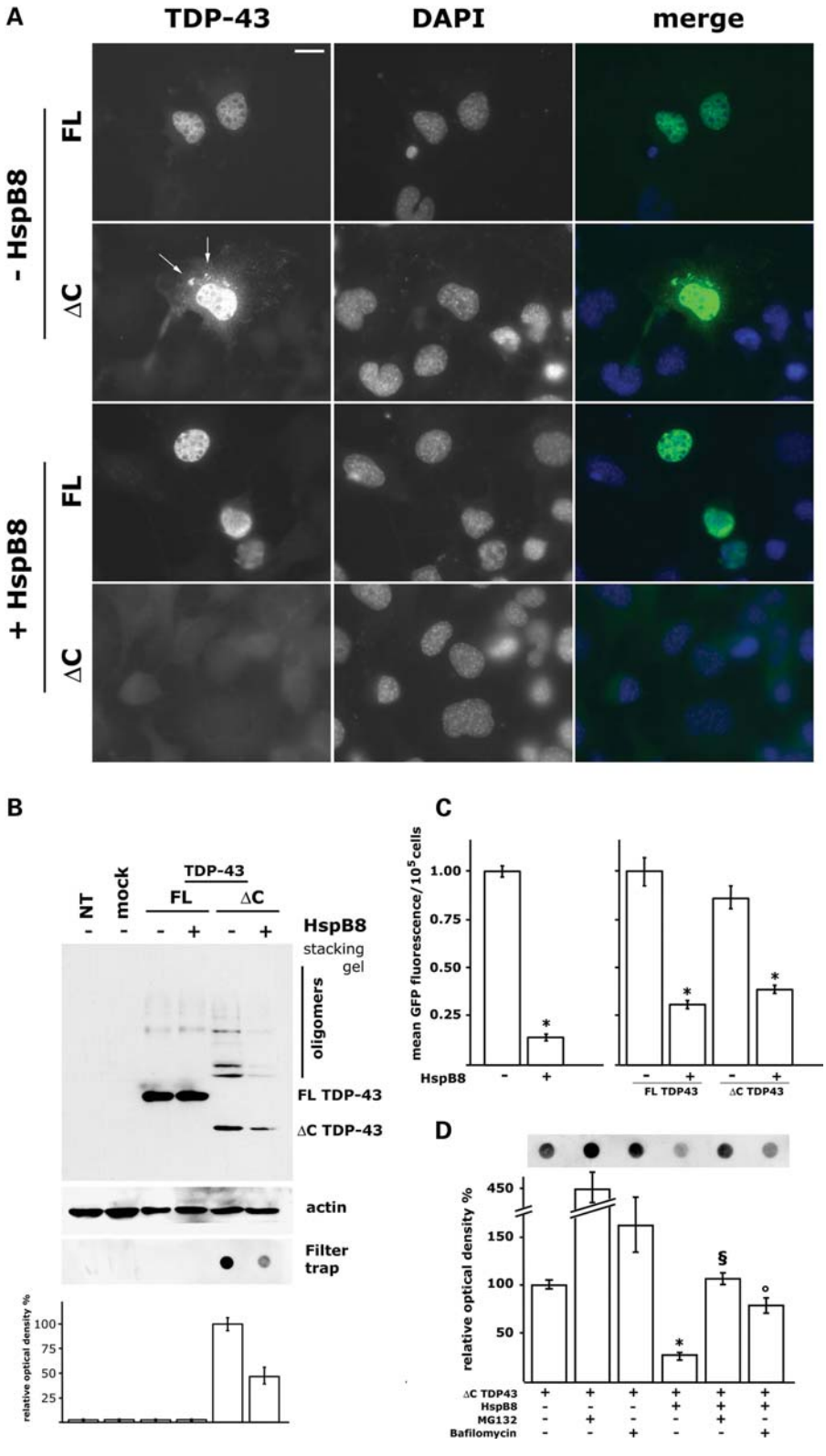

Figure 7. Effects of HspB8 on FL TDP-43 and ΔC TDP-43 subcellular localization, aggregation and solubility in motor neuronal NSC34 cells. (**A**) Immunofluorescence analysis (×40) on NSC34 cells expressing either FLAG-tagged FL TDP-43 or ΔC TDP-43 and HspB8. Arrows indicate ΔC TDP-43 cytoplasmic aggregates. Scale bar = 10 μm. (**B**) Western blot and filter retardation assays on NSC34 expressing either FLAG-tagged FL TDP-43 or ΔC TDP-43 and HspB8. FL TDP-43 = human full-length TDP-43 monomeric forms; ΔC TDP-43, human C-terminus truncated TDP-43 monomeric forms; oligomers, dimeric/high MW species of ΔC TDP-43; NT, non-transfected cells; mock, NSC34 transfected with the empty vector. The histogram represents a quantification of the filter retardation assay (from three different replicates). (**C**) Flow cytofluorimetric analysis performed on NSC34 cells expressing GFP-LC3 and either FL TDP-43 or ΔC

(2,5); TDP-43 mutations (mainly C-terminal) have been identified in ALS (4). These are all missense mutations, but one frameshift mutation creates a premature stop codon (p.Y374X) that generates a C-terminal truncated TDP-43 protein (26,27). In post-mortem samples of sALS patients, inclusions contain the TDP-43 C-terminus (2), but both N- and C-terminal TDP-43 fragments aggregate in neuronal cell cultures (28), and might be involved in triggering aberrant protein folding (28,29). The C-terminus retains TDP-43 into the nucleus, is essential for solubility and cellular localization, and its deletion results in the formation of large nuclear and cytoplasmic aggregates (29). Taking advantage of this system, we evaluated whether HspB8 counteracts TDP-43 misfolding and aggregation induced by the removal of the C-terminal region of the protein (ΔC TDP-43). The results in Figure 7A show the intracellular localization of the full-length TDP-43 (FL TDP-43), compared with ΔC TDP-43. While the FL TDP-43 was exclusively localized into nuclei, the ΔC TDP-43 was present in the nucleus (29,30) and aggregated in the cytoplasm. HspB8 did not modify the behavior of FL TPD-43, while it completely removed ΔC TDP-43 from the cells, suggesting that it could activate the degradation of the aberrant ΔC TDP-43 conformations. Moreover, ΔC TDP-43 formed oligomeric species migrating at higher M.W. that were almost completely removed by HspB8 expression (Fig. 7B). Only negligible levels of the truncated monomeric protein remained detectable. Finally, filter retardation analysis demonstrated that HspB8 over-expression also greatly reduced the total amounts of insoluble ΔC TDP-43. Overall, these data indicated that HspB8 is active also against ΔC TDP-43 involved in different types of ALS. We quantified the effect of HspB8 on autophagy using the bafilomycin-synchronized APLP protocol described above to measure, by flow cytofluorimetric analysis, the LC3 turnover also in the TDP-43 ALS model. The data (Fig. 7C) showed that HspB8 dramatically decreases the intracellular levels of LC3, in only 3 h of active APLP. As in the case of mutant SOD1, filter retardation assays demonstrated that HspB8 acts via the APLP system also in the case of TDP-43. In fact, bafilomycin treatment counteracted the HspB8-induced clearance of the insoluble species formed by the misfolded fragment of the TDP-43 proteins in cell lysates of NSC34 cells expressing the ΔC TDP-43 (Fig. 7D).

DISCUSSION

In the present study, we found that mutant G93A-SOD1 aggregates and impairs the proteasome system in a motor neuronal model of fALS represented by G93A-SOD1 NSC34 cells. The proteasome impairment correlates with an increased expression of the chaperone protein HspB8. We also found that HspB8 is already over expressed in a few lumbar motor neurons of PS tg G93A-SOD1 mice that also express high levels of mutant SOD1. This phenomenon become more evident and involves many more motor neurons, and also astrocytes, with disease progression until the ES. This is in line with previous results showing in two-dimensional immunoblot a progressive increase of detergent insoluble human SOD1 partially ubiquitinated in the spinal cord of tg G93A-SOD1 mice, but not in wtSOD1 mice (31). Thus, the expression pattern of HspB8 correlates with the progressive accumulation of the insoluble mutant SOD1 in an attempt, perhaps, to remove the misfolded protein responsible for motor neuronal cell death in these animals. Moreover, by analyzing the HspB8 effects on the biochemical properties of mutant SOD1 in motor neuronal cells, we found that HspB8 almost completely counteracts insoluble species formation, reducing aggregation of mutant SOD1. The HspB8 chaperone activity also clears monomeric mutant SOD1 from cells, possibly by assisting its degradation through intracellular degradative systems. Notably, HspB8 has only minor effects on the wtSOD1 degradation, and thus this chaperone selectively recognized only misfolded conformations. This aspect is particularly relevant in SOD1-linked fALS; in fact, the reduction of functional SOD1 enzyme might determine an intracellular loss of protection against neurotoxic-free radical species (6). With this selective mechanism, HspB8 prevents the loss of active SOD1 enzyme, exerting a second beneficial effect on motor neuronal cells. Interestingly, HspB8-induced clearance of mutant SOD1 does not necessarily require the activity of the proteasome, since insoluble species, aggregates and monomeric forms of mutant SOD1 are removed even during proteasome inhibition. Therefore, an alternative degradative pathway must be responsible for the removal of the mutant SOD1 neurotoxic species by HspB8. We found that, both in animal and cell models of fALS, the APLP system is activated in the presence of the mutant misfolded G93A-SOD1, since in both cases autophagosomes have been specifically observed using electron microscopy analysis. These data strongly agree with previous observations showing that both proteasome and autophagy remove mutant SOD1 (32), and suggested that autophagy is activated in SOD1-linked fALS mice (33,34). In our study, we demonstrated that HspB8 expression not only correlates with an increased proteasome-independent clearance of mutant G93A-SOD1, but also with a robust increase in intracellular autophagosomes and in the turnover of the autophagic marker LC3, which is degraded after APLP activation. HspB8 also heavily modifies the intracellular distribution of LC3, from a diffuse staining (soluble LC3-I form) to the typical punctate staining (lipidated LC3-II form, anchored to the autophagosome membrane to stimulate its fusion with the lysosome). Finally, we confirmed that HspB8 acts via the APLP, since the APLP inhibitor bafilomycin counteracted the HspB8-induced degradation of mutant SOD1 insoluble species. The mechanism(s) by which HspB8 activates mutant SOD1 clearance through autophagy is more clear on the basis of the present results. Several data showed

TDP-43. Cells have been synchronized at APLP for 15 h using 10 nM of bafilomycin, which was removed 3 h prior to analysis (mock versus mock+HspB8, FL TDP-43 versus FL TDP-43+HspB8, ΔC TDP-43 versus ΔC TDP-43+ HspB8, $^{*}P < 0.001$). (**D**) Filter retardation assays on NSC34 cells expressing FLAG-tagged ΔC TDP-43 in the absence or in the presence of HspB8, in the basal condition or after treatment with 10 μM of MG132 for 24 h, or 10 nM of bafilomycin for 24 h. The histogram represents a quantification of the filter retardation assay (from three different replicates) ($^{*}P < 0.001$, +HspB8 versus −HspB8; $^{\S}P < 0.001$, +Mg132+HspB8 versus +Mg132; $^{\circ}P < 0.001$, +HspB8+bafilo versus +HspB8).

that HspB8 forms stable complexes with Bag3 required to stimulate autophagy (11,12). Notably, Bag3 knock-out mice show muscular loss (35), and mutant Bag3 has been associated with muscular dystrophy and peripheral neuropathy (18). These findings suggest that HspB8, together with its partner Bag3, may play an important role for the survival of motor neurons and muscular cells. The interaction domain between HspB8 and Bag-3 has been recently fully characterized (36), and the pathway utilized by HspB8 to target misfolded proteins to the autophagic degradation has been unraveled in muscle cells (25). The HspB8 complexes with Bag-3 and subsequently recruits Hsc70 and CHIP; this heteromeric complex recognizes the misfolded protein assisted by p62 and activates autophagy (25). Interestingly, Hsc70 has been found to be highly enriched in mutant SOD1 in detergent-insoluble fractions from the spinal cord of tg fALS mice at different stages of disease (37). Finally, CHIP, a component of the HspB8/Bag3/Hsc70/CHIP, is a well-known interactor of the mutant SOD1 (38). It has also been demonstrated that ubiquitinated Hsc70 induces degradation of mutant SOD1 by interacting with CHIP (38).

The immunoprecipitation, performed using an anti-SOD1 antibody in NSC34 immortalized motor neurons with autophagosome formation blocked by 3-MA, definitely demonstrated that mutant SOD1 clearance with HspB8 is mediated by autophagy. In fact, only a small amount of HspB8 or Bag3 can be found bound to mutant SOD1 in the basal conditions, when misfolded SOD1 is probably recognized and immediately targeted to autophagic degradation. In fact, inhibition of autophagosome assembly, which prevents misfolded mutant SOD1 clearance via autophagy, leads to its accumulation in the multiheteromeric complex containing not only HspB8, but also Bag3, Hsc70 and CHIP; these proteins are all required for misfolded protein insertion into the autophagosome (25). Our data thus strongly suggest that HspB8 has a key role by acting as the first element of the entire system. These complementary data provide a molecular explanation of the HspB8 action on mutant SOD1 and reinforce the hypothesis that a reduction in the autophagic flux might be responsible for misfolded protein accumulation. Thus, HspB8 plays an essential role in motor neuronal disease, since the simple over-expression of one of the components (HspB8) of the autophagy-mediated degradative system (HspB8/Bag3/Hsc70/CHIP) seems to be sufficient to restore an active process. The HspB8 in this view has to be considered the limiting factor of the process. These data may also explain why anterior horn spinal cord motor neurons of tg ALS mice over-expressed HspB8; possibly, this is an attempt to eliminate the neurotoxic misfolded protein via autophagy, or response to proteasomal inhibition. The same mechanism can also take place in the astrocytes, which, at ES, also over-expressed HspB8.

We also found, in agreement with previous data, that TDP-43 lacking the C-terminal domain (ΔC TDP-43) mislocalized in the cell cytoplasm (28,29), generating oligomeric insoluble forms. Our data demonstrate that HspB8 completely counteracts the formation of oligomeric species of ΔC TDP-43, and greatly reduces the total amount of insoluble species of ΔC TDP-43 in motor neurons. Even in the case of TDP-43, our data proved that HspB8 activity is mediated by autophagy. These observations are in line with data showing that autophagy is involved in basal TDP-43 metabolism; in fact, autophagy inhibition increases TDP-43 accumulation, while rapamycin, an inhibitor of mTOR (a key protein in autophagy regulation), restores TDP-43 nuclear localization, preventing its cytoplasmic accumulation (39). In our study, the APLP inhibition resulted in the loss of HspB8-mediated degradation of TDP-43 insoluble species.

Thus, HspB8 chaperone activity might be implicated in the degradation of several types of neurotoxic proteins accumulating in TDP-43-positive aggregates in most of the cases of sporadic ALS, in some fALS not linked to SOD1 mutations, as well as in frontotemporal dementia (2,4,5). A screening on genes involved in fALS or sALS has demonstrated that, among others, HspB8 expression is significantly increased in autoptic lumbar spinal cord from both sALS and SOD1-linked fALS cases (40). Unfortunately, the study did not consider whether this increased HspB8 mRNA expression is confined to spinal cord motor neurons in ALS patients. Our immunohistochemical study in tg G93A-SOD1 mice spinal cord clearly indicates that HspB8 over-expression occurs in motor neuronal cells in response to mutant SOD1 accumulation. Thus, both animal model and sALS patient data strongly support the hypothesis that HspB8 might be activated in response to the aberrant behavior of mutant misfolded proteins in motor neurons, in the attempt to counteract their neurotoxicity. Interestingly, it has been recently reported that the expression in primary culture of motor neurons of the HspB8 (K141N and K141E) mutant lacking chaperone activity correlates with neurite degeneration (41), and this effect is specific for spinal cord motor neurons. HspB8 also counteracts the formation of inclusion bodies containing pre-amyloid oligomer intermediates (amyloid oligomer) of mutant HspB5 (alpha-β-crystallin), a small Hsp that causes desmin-related cardiomyopathy (DRM) (42). In this case, HspB8 significantly improves cardiac function and survival of R120G tg mice expressing the mutant HspB5 (43).

Overall, these results indicate that the pharmacological modulation of the HspB8 expression in motor neurons may have an important implication in unraveling the molecular mechanisms involved both in fALS and in sALS.

MATERIALS AND METHODS

Materials and additional methods are available in the Supplementary Material.

Plasmids

pCDNA3-wtSOD1 and pCDNA3-G93A-SOD1 express wtSOD1 and mutant G93A-SOD1 (44). pECFP-wtSOD1 and pECFP-G93A-SOD1 express wt and mutant human SOD1 tagged with cyan fluorescent protein (CFP) (6). YFPu expresses a CL1-tagged YFP, a proteasome activity reporter protein (6,16). pEGFP-wtSOD1 and pEGFP-G93A-SOD1 express the green FP (GFP)-tagged wt and mutant SOD1 (see Supplementary Material for details). pCNEO-cMyc-HspB8 expresses the rat HspB8 (from J. Landry, Canada) (45). pCIHspB8-K141N and pCIHspB8-K141E express HspB8 with Lysine 141 changed to asparagine or glutamate, respectively (from S.C., The

Netherlands) (10). pGL3-enhancer and pRL-TK are from Promega (Madison, WI, USA); pCMVβ and pEGFP-N1 are from Clontech Lab (Mountain View, CA, USA). promB8, generated in our laboratory, contains the firefly luciferase cDNA under the control of a −3000/+523 human HspB8 promoter region (see Supplementary Material for details). pFLAG-FL TDP-43 and pFLAG-ΔC TDP-43 express FLAG-tagged wt full-length human TDP-43 and a C-terminus truncated form (from E. Buratti, Italy) (29). pEGFP-LC3 expresses a GFP-tagged rat LC3 (from T. Yoshimori, Japan) (46).

Cell cultures and transfection

The immortalized motor neuronal cell line, NSC34 (14), has been routinely maintained and transfected [Lipofectamin (Invitrogen)/transferrin (Sigma) 2:1] as previously described (15).

NSC34 stable-transfected cell lines (from M.T. Carrì, Italy) express myc-tagged human wtSOD1 or G93A-SOD1 and have been routinely maintained as described by Ferri *et al*. (47).

Animals

Transgenic SOD1G93A mice on C57BL/6JOlaHsd (C57/G93A) genetic background and corresponding non-tg littermates were used. Mice were maintained as previously described (48) and according to the institutional guidelines, that are in compliance with national (D.L. no. 116, G.U. suppl. 40, 18 February 1992, Circolare No. 8, G.U., 14 July 1994) and international laws and policies (EEC Council Directive 86/609, OJ L 358, 1, 12 December 1987; NIH Guide for the Care and use of Laboratory Animals, U.S. National Research Council, 1996).

To evaluate disease stages, starting from the 14th week of age and twice a week, mice were tested for deficit in grip strength and rotarod performance by the same operator. The onset of symptoms was considered when the mice showed the first impairment in grip strength. Body weight loss was also followed. Mice have been sacrificed at the presymptomatic (PS, 12 weeks), clinical symptomatic (CS, 18 weeks on the average) and end stage (ES, 24–25 weeks on the average) of the progression of the motor dysfunction.

Immunohistochemistry on mice spinal cord sections

Sample preparation is described in the Supplementary Material. The following mice were analyzed ($n = 3$ per group and per age): non-tg, transgenic G93A-SOD1, transgenic wtSOD1 at PS, CS, ES ages of disease progression, using as primary antibodies: rabbit polyclonal antibody against HspB8 (from J. Landry, Canada; dilution 1:200), mouse monoclonal anti-human SOD1 (MBL, Japan; dilution 1:3000) and mouse monoclonal anti-GFAP to detect astrocytes (Invitrogen, 1:2500), revealed by secondary biotinylated antisera (goat anti-rabbit and horse anti-mouse, Vector, 1:200) and the Avidin-Biotin-peroxidase Complex (ABC, Vector), using diaminobenzidine as chromogen.

For immunofluorescence secondary antibodies conjugated to different fluorochromes (goat anti-rabbit Alexa 488, Invitrogen, 1:200; donkey anti-mouse CY3, Jackson, 1:1400) were used to visualize HspB8, SOD1 and GFAP, whereas the biotinylated *Lycopersicon esculentum* agglutinin (LEA, 1:2000; Vector Laboratories) revealed by streptavidin-RedX (Invitrogen) was used for the detection of microglia. Samples were analyzed with a TCS NT confocal laser scanning microscope (Leica Lasertecknik GmbH, Heidelberg, Germany) equipped with a 75 mW Kripton/Argon mixed gas laser.

Control sections processed without the primary antisera gave no immunostaining.

Fluorescence, immunofluorescence and microscopy on NSC34 cells

Sample preparation is described in the Supplementary Material. To analyze SOD1s, TDP-43s, HspB8 and ubiquitin [primary antibodies: mouse monoclonal anti-FLAG (Sigma), 1:200 in milk, rabbit polyclonal anti-HspB8 antibody, 1:200 in milk, mouse monoclonal anti-ub (Santa Cruz), 1:200 in milk; secondary antibody: Alexa 488 anti-rabbit, Alexa 488 anti-mouse and Alexa 594 anti-mouse (Invitrogen), 1:1000 in milk] were used an Axiovert 200 microscope (Zeiss Instr., Oberkochen, Germany) combined with a Photometric CoolSnap CCD camera (Ropper Scientific, Trenton, NJ, USA). Images were processed using Metamorph software (Universal Imaging, Downingtown, PA, USA).

Western blot analysis and filter retardation assay

Western blot analysis has been performed as previously described (6) and details are summarized in Supplementary Material. The following primary and secondary antibodies were used: (i) for YFPu, mouse monoclonal anti-GFP (Zymed, San Francisco, CA, USA; 1:1000 in milk); (ii) for SOD1, rabbit polyclonal anti-Cu/Zn superoxide dismutase SOD1 (SOD-100; Assay Designs; 1:1000 in milk); (iii) for TDP-43, mouse monoclonal anti-FLAG (Sigma; 1:1000 in milk), (iv) for Actin, goat polyclonal anti-Actin (Actin I-19; Santa Cruz; 1:1000 in milk); (v) the rabbit polyclonal antibody against HspB8 (from J. Landry; 1:1000 in milk) or (vi) the mouse monoclonal c-Myc (9E10) (Santa Cruz; 1:1000 in milk) for HspB8; (vii) for GFP-SOD1s, the peroxidase-labeled goat Anti-GFP (Vector Laboratories; 1:5000 in TBS-T); (ix) the mouse monoclonal anti-ub (Santa Cruz; 1:1000 in milk) for ubiquitin; goat anti-rabbit, goat anti-mouse and donkey anti-goat peroxidase-conjugated secondary antibodies (Santa Cruz; 1:5000 in TBS-T).

Filter retardation assay was performed on a 0.2 μm cellulose acetate membrane (Whatman, Dassel, Germany) as previously described (6) and details are summarized in Supplementary Material. Slot blots were probed as described for western blots. The optical intensity of the spots was analyzed using NIH ImageJ software.

mRNA expression analysis

RT–PCR and real-time PCR have been performed as previously described (49–51) and details are summarized in Supplementary Material. Total RNA from lumbar spinal cord of mice was obtained following ethically approved protocols. Each sample was analyzed in duplicate and HspB8 values were then normalized with those of GAPDH.

Immunoprecipitation analysis

Sample preparation is described in the Supplementary Material. The antibodies utilized to recognize the multiheteromeric complex of SOD1, HspB8 and other proteins were the following: anti-Cu/Zn superoxide dismutase SOD1 (SOD-100; Assay Designs) rabbit polyclonal antibody for immunoprecipitation and SOD1 detection in western blot, anti-c-myc (9E10; Santa Cruz) mouse monoclonal antibody recognizing transfected HspB8, anti-Bag3 (Abcam) rabbit polyclonal antibody, anti-Hsc70 (Stressgen) rabbit polyclonal antibody, anti-CHIP (Calbiochem) rabbit polyclonal antibody.

Transcriptional activity

Transcriptional activity has been performed as previously described (20) using either the LucLite Kit from Perkin Elmer (Waltham, MA, USA) normalized with β-galactosidase assay or the Dual Luciferase Assay System (Promega) (see Supplementary Material for details).

Cytofluorimetric analysis

Cytofluorimetric analysis was performed on GFP-LC3 or GFP-G93A-SOD1 transfected NSC34 cells (see Supplementary Material for details). GFP fluorescence was detected using FACS Calibur (BD Pharmingen) and results analyzed using CellQuest (BD Pharmigen) software.

Statistical analysis

Statistical analysis has been performed using one-tailed Student's *t*-test for two group comparisons and one-way ANOVA for three or more group comparisons using the PRISM software (GraphPad, San Diego, CA, USA).

SUPPLEMENTARY MATERIAL

Supplementary Material is available at *HMG* online.

ACKNOWLEDGEMENTS

We thank N.R. Cashman (Department of Medicine, Center for Research in Neurodegenerative Diseases, Sunnybrook and Women's College Health Sci Centre, University of Toronto, Ontario, Canada) for NSC34 cells, Maria Teresa Carrì (University of Roma 'Tor Vergata', Italy) for the stable transfected SOD1_NSC34 cell lines, J. Landry (Centre of Recherche Cancerologie, University of Laval, Canada) for pCNEO-cMyc-HspB8 and anti-HspB8 antibody, T. Yoshimori (Department of Cellular Regulation, Research Institute for Microbial Diseases, Osaka University of Osaka, Japan) for pEGFP-LC3, E. Buratti (International Centre for Genetic Engineering and Biotechnology, AREA Science Park, Padriciano, Trieste, Italy) for pFLAG-FL TDP-43 and pFLAG-ΔC TDP-43.

Conflict of Interest statement. None declared.

FUNDING

This work was supported by Telethon, Italy (grant no. GGP06063 to A.P., C.B., S.D.B. and GGP07063 to A.P.); Italian Ministry of University and Research; Italian Ministry of Labour, Health and Social Affairs (grant no. 2007-36 to A.P.; 2008-15 to A.P. and convenzione Fondazione Mondino/UNIMI); Universita' degli Studi di Milano and Fondazione CARIPLO (grant no. 2008-2307 to A.P.); Fondation Thierry Latran, France (2009 to A.P.). Confocal microscopy was carried out at the Centro Interdipartimentale di Microscopia Avanzata (CIMA) of the University of Milan.

REFERENCES

1. Bendotti, C. and Carri, M.T. (2004) Lessons from models of SOD1-linked familial ALS. *Trends Mol. Med.*, **10**, 393–400.
2. Neumann, M., Sampathu, D.M., Kwong, L.K., Truax, A.C., Micsenyi, M.C., Chou, T.T., Bruce, J., Schuck, T., Grossman, M., Clark, C.M. *et al.* (2006) Ubiquitinated TDP-43 in frontotemporal lobar degeneration and amyotrophic lateral sclerosis. *Science*, **314**, 130–133.
3. Rosen, D.R., Siddique, T., Patterson, D., Figlewicz, D.A., Sapp, P., Hentati, A., Donaldson, D., Goto, J., O'Regan, J.P., Deng, H.X. *et al.* (1993) Mutations in Cu/Zn superoxide dismutase gene are associated with familial amyotrophic lateral sclerosis. *Nature*, **362**, 59–62.
4. Kabashi, E., Valdmanis, P.N., Dion, P., Spiegelman, D., McConkey, B.J., Vande Velde, C., Bouchard, J.P., Lacomblez, L., Pochigaeva, K., Salachas, F. *et al.* (2008) TARDBP mutations in individuals with sporadic and familial amyotrophic lateral sclerosis. *Nat. Genet.*, **40**, 572–574.
5. Sreedharan, J., Blair, I.P., Tripathi, V.B., Hu, X., Vance, C., Rogelj, B., Ackerley, S., Durnall, J.C., Williams, K.L., Buratti, E. *et al.* (2008) TDP-43 mutations in familial and sporadic amyotrophic lateral sclerosis. *Science*, **319**, 1668–1672.
6. Sau, D., De Biasi, S., Vitellaro-Zuccarello, L., Riso, P., Guarnieri, S., Porrini, M., Simeoni, S., Crippa, V., Onesto, E., Palazzolo, I. *et al.* (2007) Mutation of SOD1 in ALS: a gain of a loss of function. *Hum. Mol. Genet.*, **16**, 1604–1618.
7. Shaw, B.F. and Valentine, J.S. (2007) How do ALS-associated mutations in superoxide dismutase 1 promote aggregation of the protein? *Trends Biochem. Sci.*, **32**, 78–85.
8. Irobi, J., Van Impe, K., Seeman, P., Jordanova, A., Dierick, I., Verpoorten, N., Michalik, A., De Vriendt, E., Jacobs, A., Van Gerwen, V. *et al.* (2004) Hot-spot residue in small heat-shock protein 22 causes distal motor neuropathy. *Nat. Genet.*, **36**, 597–601.
9. Tang, B.S., Zhao, G.H., Luo, W., Xia, K., Cai, F., Pan, Q., Zhang, R.X., Zhang, F.F., Liu, X.M., Chen, B. *et al.* (2005) Small heat-shock protein 22 mutated in autosomal dominant Charcot–Marie–Tooth disease type 2L. *Hum. Genet.*, **116**, 222–224.
10. Carra, S., Sivilotti, M., Chavez Zobel, A.T., Lambert, H. and Landry, J. (2005) HspB8, a small heat shock protein mutated in human neuromuscular disorders, has in vivo chaperone activity in cultured cells. *Hum. Mol. Genet.*, **14**, 1659–1669.
11. Carra, S., Seguin, S.J., Lambert, H. and Landry, J. (2008) HspB8 chaperone activity toward poly(Q)-containing proteins depends on its association with Bag3, a stimulator of macroautophagy. *J. Biol. Chem.*, **283**, 1437–1444.
12. Carra, S., Brunsting, J.F., Lambert, H., Landry, J. and Kampinga, H.H. (2009) HspB8 participates in protein quality control by a non-chaperone-like mechanism that requires eIF2{alpha} phosphorylation. *J. Biol. Chem.*, **284**, 5523–5532.
13. Poletti, A. (2004) The polyglutamine tract of androgen receptor: from functions to dysfunctions in motor neurons. *Front. Neuroendocrinol.*, **25**, 1–26.
14. Cashman, N.R., Durham, H.D., Blusztajn, J.K., Oda, K., Tabira, T., Shaw, I.T., Dahrouge, S. and Antel, J.P. (1992) Neuroblastoma x spinal cord (NSC) hybrid cell lines resemble developing motor neurons. *Dev. Dyn.*, **194**, 209–221.
15. Simeoni, S., Mancini, M.A., Stenoien, D.L., Marcelli, M., Weigel, N.L., Zanisi, M., Martini, L. and Poletti, A. (2000) Motoneuronal cell death is

not correlated with aggregate formation of androgen receptors containing an elongated polyglutamine tract. *Hum. Mol. Genet.*, **9**, 133–144.
16. Rusmini, P., Sau, D., Crippa, V., Palazzolo, I., Simonini, F., Onesto, E., Martini, L. and Poletti, A. (2007) Aggregation and proteasome: the case of elongated polyglutamine aggregation in spinal and bulbar muscular atrophy. *Neurobiol. Aging*, **28**, 1099–1111.
17. Evgrafov, O.V., Mersiyanova, I., Irobi, J., Van Den Bosch, L., Dierick, I., Leung, C.L., Schagina, O., Verpoorten, N., Van Impe, K., Fedotov, V. *et al.* (2004) Mutant small heat-shock protein 27 causes axonal Charcot–Marie–Tooth disease and distal hereditary motor neuropathy. *Nat. Genet.*, **36**, 602–606.
18. Selcen, D., Muntoni, F., Burton, B.K., Pegoraro, E., Sewry, C., Bite, A.V. and Engel, A.G. (2009) Mutation in BAG3 causes severe dominant childhood muscular dystrophy. *Ann. Neurol.*, **65**, 83–89.
19. Gamerdinger, M., Hajieva, P., Kaya, A.M., Wolfrum, U., Hartl, F.U. and Behl, C. (2009) Protein quality control during aging involves recruitment of the macroautophagy pathway by BAG3. *EMBO J.*, **28**, 889–901.
20. Vismara, G., Simonini, F., Onesto, E., Bignamini, M., Miceli, V., Martini, L. and Poletti, A. (2009) Androgens inhibit androgen receptor promoter activation in motor neurons. *Neurobiol. Dis.*, **33**, 395–404.
21. Williams, A., Jahreiss, L., Sarkar, S., Saiki, S., Menzies, F.M., Ravikumar, B. and Rubinsztein, D.C. (2006) Aggregate-prone proteins are cleared from the cytosol by autophagy: therapeutic implications. *Curr. Top. Dev. Biol.*, **76**, 89–101.
22. Fontanella, B., Birolo, L., Infusini, G., Cirulli, C., Marzullo, L., Pucci, P., Turco, M.C. and Tosco, A. (2010) The co-chaperone BAG3 interacts with the cytosolic chaperonin CCT: new hints for actin folding. *Int. J. Biochem. Cell Biol.*, **42**, 641–650.
23. McCollum, A.K., Casagrande, G. and Kohn, E.C. (2010) Caught in the middle: the role of Bag3 in disease. *Biochem. J.*, **425**, e1–e3.
24. Rubinsztein, D.C., Cuervo, A.M., Ravikumar, B., Sarkar, S., Korolchuk, V., Kaushik, S. and Klionsky, D.J. (2009) In search of an 'autophagomometer'. *Autophagy*, **5**, 585–589.
25. Arndt, V., Dick, N., Tawo, R., Dreiseidler, M., Wenzel, D., Hesse, M., Furst, D.O., Saftig, P., Saint, R., Fleischmann, B.K. *et al.* (2010) Chaperone-assisted selective autophagy is essential for muscle maintenance. *Curr. Biol.*, **20**, 143–148.
26. Lagier-Tourenne, C. and Cleveland, D.W. (2009) Rethinking ALS: the FUS about TDP-43. *Cell*, **136**, 1001–1004.
27. Daoud, H., Valdmanis, P.N., Kabashi, E., Dion, P., Dupre, N., Camu, W., Meininger, V. and Rouleau, G.A. (2009) Contribution of TARDBP mutations to sporadic amyotrophic lateral sclerosis. *J. Med. Genet.*, **46**, 112–114.
28. Nonaka, T., Kametani, F., Arai, T., Akiyama, H. and Hasegawa, M. (2009) Truncation and pathogenic mutations facilitate the formation of intracellular aggregates of TDP-43. *Hum. Mol. Genet.*, **18**, 3353–3364.
29. Ayala, Y.M., Zago, P., D'Ambrogio, A., Xu, Y.F., Petrucelli, L., Buratti, E. and Baralle, F.E. (2008) Structural determinants of the cellular localization and shuttling of TDP-43. *J. Cell Sci.*, **121**, 3778–3785.
30. Nonaka, T., Arai, T., Buratti, E., Baralle, F.E., Akiyama, H. and Hasegawa, M. (2009) Phosphorylated and ubiquitinated TDP-43 pathological inclusions in ALS and FTLD-U are recapitulated in SH-SY5Y cells. *FEBS Lett.*, **583**, 394–400.
31. Basso, M., Massignan, T., Samengo, G., Cheroni, C., De Biasi, S., Salmona, M., Bendotti, C. and Bonetto, V. (2006) Insoluble mutant SOD1 is partly oligoubiquitinated in amyotrophic lateral sclerosis mice. *J. Biol. Chem.*, **281**, 33325–33335.
32. Kabuta, T., Suzuki, Y. and Wada, K. (2006) Degradation of amyotrophic lateral sclerosis-linked mutant Cu,Zn-superoxide dismutase proteins by macroautophagy and the proteasome. *J. Biol. Chem.*, **281**, 30524–30533.
33. Morimoto, N., Nagai, M., Ohta, Y., Miyazaki, K., Kurata, T., Morimoto, M., Murakami, T., Takehisa, Y., Ikeda, Y., Kamiya, T. *et al.* (2007) Increased autophagy in transgenic mice with a G93A mutant SOD1 gene. *Brain Res.*, **1167**, 112–117.
34. Li, L., Zhang, X. and Le, W. (2008) Altered macroautophagy in the spinal cord of SOD1 mutant mice. *Autophagy*, **4**, 290–293.
35. Homma, S., Iwasaki, M., Shelton, G.D., Engvall, E., Reed, J.C. and Takayama, S. (2006) BAG3 deficiency results in fulminant myopathy and early lethality. *Am. J. Pathol.*, **169**, 761–773.
36. Fuchs, M., Poirier, D.J., Seguin, S.J., Lambert, H., Carra, S., Charette, S.J. and Landry, J. (2010) Identification of the key structural motifs involved in HspB8/HspB6-Bag3 interaction. *Biochem. J.*, **425**, 245–255.
37. Basso, M., Samengo, G., Nardo, G., Massignan, T., D'Alessandro, G., Tartari, S., Cantoni, L., Marino, M., Cheroni, C., De Biasi, S. *et al.* (2009) Characterization of detergent-insoluble proteins in ALS indicates a causal link between nitrative stress and aggregation in pathogenesis. *PLoS ONE*, **4**, e8130.
38. Urushitani, M., Kurisu, J., Tateno, M., Hatakeyama, S., Nakayama, K., Kato, S. and Takahashi, R. (2004) CHIP promotes proteasomal degradation of familial ALS-linked mutant SOD1 by ubiquitinating Hsp/Hsc70. *J. Neurochem.*, **90**, 231–244.
39. Caccamo, A., Majumder, S., Deng, J.J., Bai, Y., Thornton, F.B. and Oddo, S. (2009) Rapamycin rescues TDP-43 mislocalization and the associated low molecular weight neurofilament instability. *J. Biol. Chem.*, **284**, 27416–27424.
40. Anagnostou, G., Akbar, M.T., Paul, P., Angelinetta, C., Steiner, T.J. and de Belleroche, J. (2010) Vesicle associated membrane protein B (VAPB) is decreased in ALS spinal cord. *Neurobiol. Aging*, **31**, 969–985.
41. Irobi, J., Almeida-Souza, L., Asselbergh, B., De Winter, V., Goethals, S., Dierick, I., Krishnan, J., Timmermans, J.P., Robberecht, W., De Jonghe, P. *et al.* (2010) Mutant HSPB8 causes motor neuron specific neurite degeneration. *Hum. Mol. Genet*., doi:10.1093/hmg/ddq234.
42. Sanbe, A., Yamauchi, J., Miyamoto, Y., Fujiwara, Y., Murabe, M. and Tanoue, A. (2007) Interruption of CryAB-amyloid oligomer formation by HSP22. *J. Biol. Chem.*, **282**, 555–563.
43. Sanbe, A., Daicho, T., Mizutani, R., Endo, T., Miyauchi, N., Yamauchi, J., Tanonaka, K., Glabe, C. and Tanoue, A. (2009) Protective effect of geranylgeranylacetone via enhancement of HSPB8 induction in desmin-related cardiomyopathy. *PLoS ONE*, **4**, e5351.
44. Tortarolo, M., Crossthwaite, A.J., Conforti, L., Spencer, J.P., Williams, R.J., Bendotti, C. and Rattray, M. (2004) Expression of SOD1 G93A or wild-type SOD1 in primary cultures of astrocytes down-regulates the glutamate transporter GLT-1: lack of involvement of oxidative stress. *J. Neurochem.*, **88**, 481–493.
45. Chavez Zobel, A.T., Loranger, A., Marceau, N., Theriault, J.R., Lambert, H. and Landry, J. (2003) Distinct chaperone mechanisms can delay the formation of aggresomes by the myopathy-causing R120G alphaB-crystallin mutant. *Hum. Mol. Genet.*, **12**, 1609–1620.
46. Kabeya, Y., Mizushima, N., Ueno, T., Yamamoto, A., Kirisako, T., Noda, T., Kominami, E., Ohsumi, Y. and Yoshimori, T. (2000) LC3, a mammalian homologue of yeast Apg8p, is localized in autophagosome membranes after processing. *EMBO J.*, **19**, 5720–5728.
47. Ferri, A., Cozzolino, M., Crosio, C., Nencini, M., Casciati, A., Gralla, E.B., Rotilio, G., Valentine, J.S. and Carri, M.T. (2006) Familial ALS-superoxide dismutases associate with mitochondria and shift their redox potentials. *Proc. Natl Acad. Sci. USA*, **103**, 13860–13865.
48. Pizzasegola, C., Caron, I., Daleno, C., Ronchi, A., Minoia, C., Carri, M.T. and Bendotti, C. (2009) Treatment with lithium carbonate does not improve disease progression in two different strains of SOD1 mutant mice. *Amyotroph. Lateral Scler.*, **10**, 221–228.
49. Pozzi, P., Bendotti, C., Simeoni, S., Piccioni, F., Guerini, V., Marron, T.U., Martini, L. and Poletti, A. (2003) Androgen 5-alpha-reductase type 2 is highly expressed and active in rat spinal cord motor neurones. *J. Neuroendocrinol.*, **15**, 882–887.
50. Marron, T.U., Guerini, V., Rusmini, P., Sau, D., Brevini, T.A.L., Martini, L. and Poletti, A. (2005) Androgen-induced neurite outgrowth is mediated by neuritin in motor neurones. *J. Neurochem.*, **92**, 10–20.
51. Poletti, A., Rampoldi, A., Piccioni, F., Volpi, S., Simeoni, S., Zanisi, M. and Martini, L. (2001) 5alpha-reductase type 2 and androgen receptor expression in gonadotropin releasing hormone GT1-1 cells. *J. Neuroendocrinol.*, **13**, 353–357.